# ACTIVE CONTROL OF FULLY DEVELOPED TURBULENT CHANNEL FLOWS

TADAHISA TERAO
DEPARTMENT OF MECHANICAL ENGINEERING, ROYAL INSTITUTE OF TECHNOLOGY
100-44 STOCKHOLM, SWEDEN

ARNE V. JOHANSSON
DEPARTMENT OF MECHANICAL ENGINEERING, ROYAL INSTITUTE OF TECHNOLOGY
100-44 STOCKHOLM, SWEDEN

## ABSTRACT

Active feedback control strategies are performed with the aim of reducing skin-friction drag and the ultimate goal of inducing relaminarization by blowing and suction on the boundary walls of turbulent channel flows. Direct numerical simulation enabled us to detect the wall normal velocity at various distances from the wall and impose blowing and suction with various values of the amplitude and phase. Some strategies were successful to achieve up to 30% drag reduction with suitable combinations of sensing location, amplitude and phase. In this study, we also investigated the effect of control scheme on the passive scalar field, induced by a constant temperature difference between the walls.

## INTRODUCTION

It has been recognized that the coherent structures in turbulent boundary layers play a significant role for skin-friction drag (Robinson 1991; Kasagi et al. 1995), but the underlying mechanism has not been fully understood. The control of turbulence is a challenging research topic and has great potential for engineering application. A number of studies have been carried out during the past few years, especially by means of direct numerical simulation (DNS), for the purpose of reducing drag through active turbulence control.

Control of turbulent boundary layers with uniform blowing and suction were performed by Choi et al. (1997) and Sumitani and Kasagi (1995). The results from these studies indicate that the uniform blowing from the wall can decrease the skin friction and increase the turbulent intensities, while a uniform suction has nearly opposite effect. Choi et al. (1994) devised feedback control schemes for active cancellation of the effect of near-wall vortices in turbulent channel flows. They observed the wall-normal velocity at different distances from the wall and imposed an equal normal velocity control on the walls in the opposite direction, resulting in a maximum suppression of the mean drag by 25% with sensing location at about $y^+ \approx 10$. They also found the drag increase with sensing location further from the wall ($y^+ \approx 26$). Hammond et al.(1998) explains this significant difference in drag behavior by establishing the concept of "virtual wall", i.e. when the sensing location is fairly close to the wall, a plane that has approximately no through-flow is formed half-way between the detection plane and the wall, which reduces vertical transport of streamwise momentum near the wall and leads to drag reduction. On the other hand, a detection plane far away from the wall fails to form this virtual wall and allows high momentum fluid to be drawn into the region between the detection plane and the wall, resulting in drag increase.

The theory of stochastically forced non-normal systems by Farrell and Ioannou (1996) gives another explanation that such opposing control with a detection plane far away from the wall can still attenuate two-dimensional roll perturbation but enhance three-dimensional oblique perturbations. Unfortunately, our results obtained by controlling a narrow range of wave numbers did not agree with this theory.

In our present study, we implemented this active feedback control scheme, with a 'sensor' that detects the wall-normal velocity component and an 'actuator' to impose blowing and suction with chosen amplitude and phase over the whole boundary walls to explore the optimization of this turbulent control strategy.

## FORMULATION OF THE CONTROL SCHEME

The problem considered here is fully developed turbulent channel flow. The governing equations for the velocity field are the incompressible Navier-Stokes equation and continuity equation with no-slip boundary condition.

$$\frac{\partial u_i}{\partial t} + u_j \frac{\partial u_i}{\partial x_j} = -\frac{\partial p}{\partial x_i} + \frac{1}{Re_c}\nabla^2 u_i \tag{1}$$

$$\frac{\partial u_i}{\partial x_i} = 0 \tag{2}$$

$$\widehat{u_i}|_{y=\pm 1} = C\widehat{u_2}|_{y=\pm y_d}\delta_{i2} \tag{3}$$

The terms were non-dimensionalized by the centerline velocity of the unmanipulated channel $U_c$ and the channel half-height h. The Reynolds number is defined as $Re_c \equiv \frac{U_c h}{\nu}$. $x_i$(i=1,2,3) = (x,y,z) denote streamwise, wall-normal, and spanwise directions respectively, and $(u_1, u_2, u_3)$ =(u,v,w) are the respective velocities. Eq.(3) describes the boundary condition for the wall-normal velocity, which is used as the control input, where hat denotes Fourier transform, and $u_i|_{y=\pm 1}$ and $u_i|_{y=\pm y_d}$ are the velocity components at the wall and the detection plane respectively. $C = |C|e^{i\Theta}$ is a complex constant with amplitude $|C|$ and phase $\Theta$ , and opposing control (Choi et al. 1994, Hammond et al. 1998) can be implemented by putting $|C| = 1$ and $\Theta = \pi$. We define $Y^+$ as the distance between the detection plane and the wall scaled by wall variables (viscosity and friction velocity, $u_\tau$). In our computation, the position of the detection plane was shifted at each time step to keep $Y^+$ constant at each wall throughout the calculation.

With buoyancy effects neglected, the temperature field can be described by a passive scalar equation.

$$\frac{\partial \theta}{\partial t} + u_j \frac{\partial \theta}{\partial x_j} = \frac{1}{PrRe_c}\nabla^2 \theta \tag{4}$$

$$\theta_{y=1} = 1 \quad \theta_{y=-1} = 0 \tag{5}$$

The temperature $\theta$ is normalized by its difference between the two walls, and the Prandtl number Pr was kept at unity in this study.

## NUMERICAL PROCEDURE

The computations were performed with pseudo spectral methods with Fourier representation in the streamwise(x) and spanwise(z) directions and Chebyshev representation in the wall-normal direction. The numerical methods used in our study is nearly the same as that of Kim et al.(1987) except that we employed the

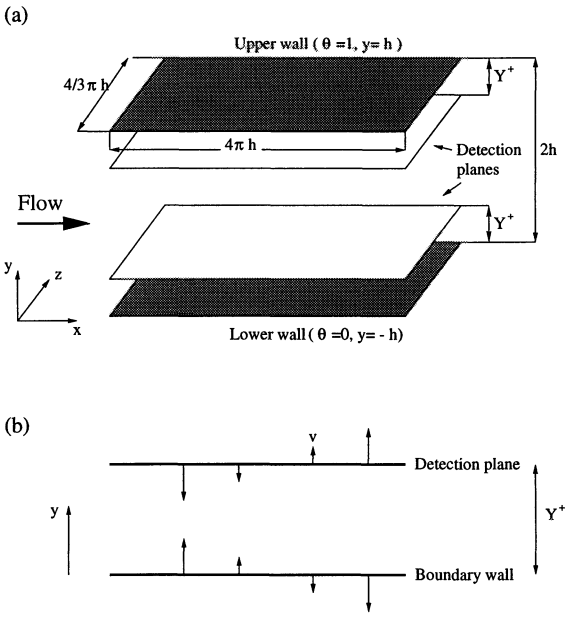


Figure 1: (a): Computational domain and coordinate system (b): schematic diagram for opposing-control ($C = -1$) case

Chebyshev integration method (Greengaard 1988) for wall-normal direction instead of Chebyshev tau method (Lanczos 1956; Gottlieb and Orszag 1977). The computational domain is set to be $(4\pi h \times 2h \times \frac{4}{3}\pi h)$ in the x, y and z directions respectively which is the same size as the one by Choi et al. (1994). First, the calculation was made at $Re_c = 1800$ with (32,65,32) spectral modes. This coarse grid allowed us to test many different control strategies, which would otherwise have required excessive computer resources.

The most successful opposing-control($C = -1$) case was repeated with (128,129,128) spectral modes at $Re_c = 3300$, from which temperature statistics and the contour plots of enstrophy were also obtained. Only with this case, a third-order Runge-Kutta method, instead of Adams-Bashforth method was applied as a time advancement scheme for non-linear terms, by which a larger computational time step can be used. The condition of constant mass flux was imposed by the continuity equation. The statistics shown in this paper were taken after a sufficiently long time to obtain stationary conditions. Since there consists few interactions between the two opposing walls, the two halves of the channel behave almost independently. Statistics are below represented by half of the channel.

## RESULTS AND DISCUSSION

Figs. 2-4 show time history of the friction Reynolds number, $Re_\tau$ with different detection planes, ampli-

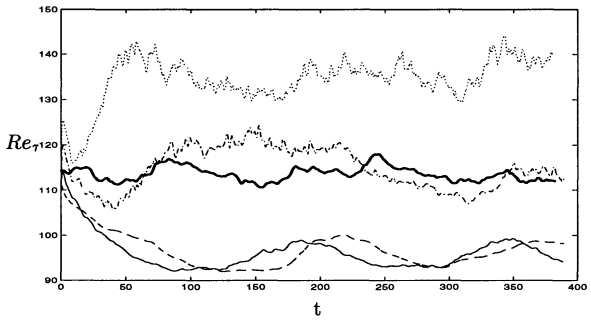


Figure 2: Time history of the friction Reynolds number with different detection planes: solid thick line, unmanipulated; dashed line, $Y^+ = 10$; solid line, $Y^+ = 15$; dash-dotted, $Y^+ = 20$; dotted, $Y^+ = 25$

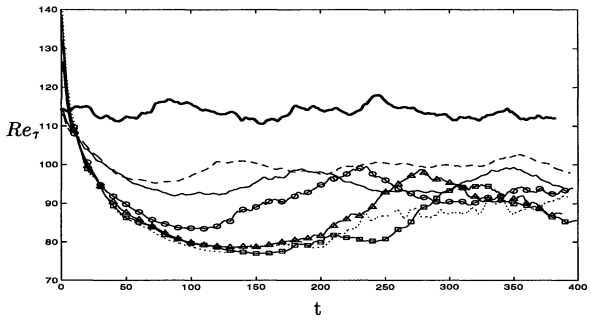


Figure 3: Time history of the friction Reynolds number at the detection plane, $Y^+ = 15$ with different amplitudes: solid thick line, unmanipulated; dashed line, $|C| = 0.5$; solid line, $|C| = 1$; circle, $|C| = 2$; triangle, $|C| = 3$; square, $|C| = 5$; dotted, $|C| = 10$

tudes, and phases, respectively. For each graph, solid thick line denotes the unmanipulated case, which shows $Re_\tau$ fluctuating around 114, and solid line represents the opposing control at $Y^+ = 15$. The time is non-dimensionalized by $U_c$ and h. The same initial velocity field with $Re_\tau \approx 114$ was employed for all cases, and some cases with larger control input has a transient increase of $Re_\tau$ immediately after the application of control input. In Fig.2, four different opposing controlled cases are represented, which agree well with previous works. The most successful drag reduction occurs with $Y^+ \approx 10$ to 15, by about 30 %. This drag reduction rate is slightly larger compared to the rate obtained by Hammond et al. (1998). We can also observe a fairly clear time-cycle for the fluctuating $Re_\tau$ in these cases. This can be related to a reduction in size of the coherent structures as compared to the unmanipulated case. These appear quasi-periodically in time even if the control input from the walls is continuously employed, and a slight shift of the detection plane leads to a phase shift of this variation. At the location $Y^+ \approx 20$, $Re_\tau$ averaged in time is almost the same as for the unmanipulated case. Here the larger amplitude of control input contributes significantly to the turbulent energy near

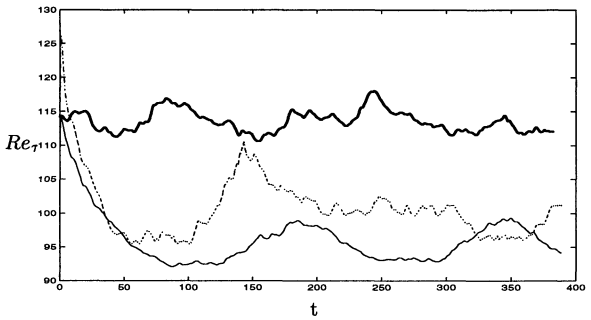


Figure 4: Time history of the friction Reynolds number at the detection plane, $Y^+ = 15$: solid thick line, unmanipulated; solid line $\Theta = \Pi$ ; dash-dotted $\Theta = \frac{\Pi}{2}$

the walls through formation of induced 'secondary' vortex structures near the walls. We can also observe a low frequency variation of $Re_\tau$ in this case. For $Y^+ \approx 25$ the drag increase is about 40 %, and $Re_\tau$ reaches a nearly stable state around 140.

Fig. 3 shows the effect of various amplitudes with the same detection point , at $Y^+ = 15$, and phase $\Theta = \Pi$. For larger amplitudes than unity, firstly, within a short time after the control is applied, an enhanced drag reduction can be observed. This indicates the larger amplitudes can counteract the sweep motion more effectively, but for large times the $Re_\tau$ values are nearly the same for the different control input amplitudes. This is also true of the case with $|C| = 100$ which is not shown here.

Fig. 4 also shows the case with $\Theta = \frac{\Pi}{2}$ along with the opposing control case at the detection point $Y^+ = 15$. The $\Theta = \frac{\Pi}{2}$ case has a peak of $Re_\tau$ at $t \approx 140$ which is almost as high as the $Re_\tau$ value for the unmanipulated case. Thereafter it tends to a value close to that of opposing control. At this stable state, the phase does not seem to be a significant factor anymore.

The opposing-controlled turbulence intensities are shown in Figs.5 and 6, with various detection planes and amplitudes. Turbulence intensities are non-dimensionalized by the mean friction velocity of the unmanipulated flow. Solid line denotes the unmanipulated case and dashed line represents opposing control with $Y^+ = 15$. In Fig.5, it can be observed that the turbulence intensities are not significantly attenuated near the center of the channel, and may even be slightly increased. For all the components, the maximum peak value is substantially reduced, which means that the active control strategy with blowing and suction on the walls dominantly affects the near wall region. In addition, the outward shift of the curves for all components indicate that the 'virtual origin' of the boundary layer is displaced and the sublayer is thickened (Choi et al. 1994). For the streamwise component, a new smaller peak can be noted, and this secondary peak becomes larger as the detection plane is moved away from the wall, and at $Y^+ = 25$, which is not shown here, this

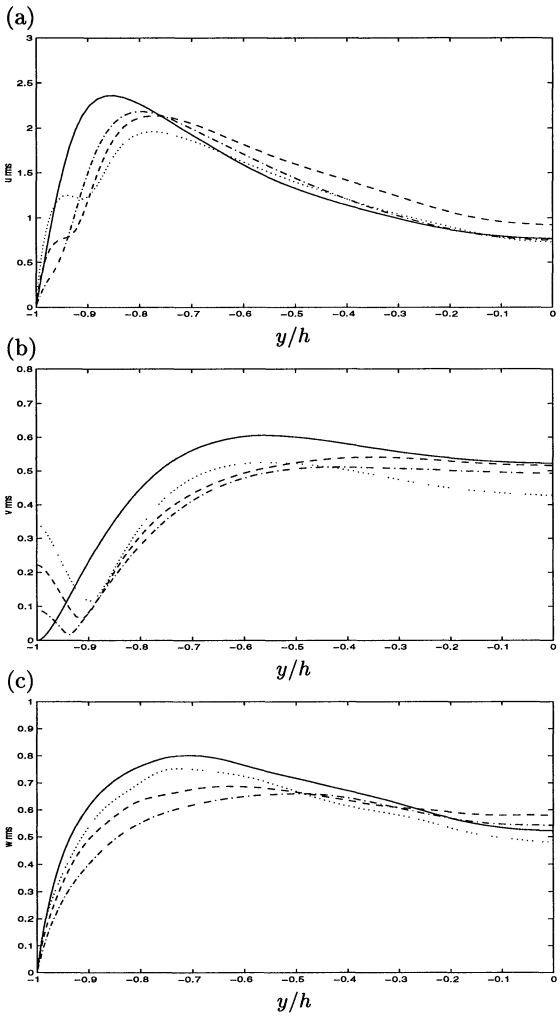


Figure 5: Turbulence intensities with different detection planes: (a) streamwise, (b) wall-normal, (c) spanwise component: solid, unmanipulated; dash-dotted, $Y^+ = 10$; dashed $Y^+ = 15$; dotted $Y^+ = 20$

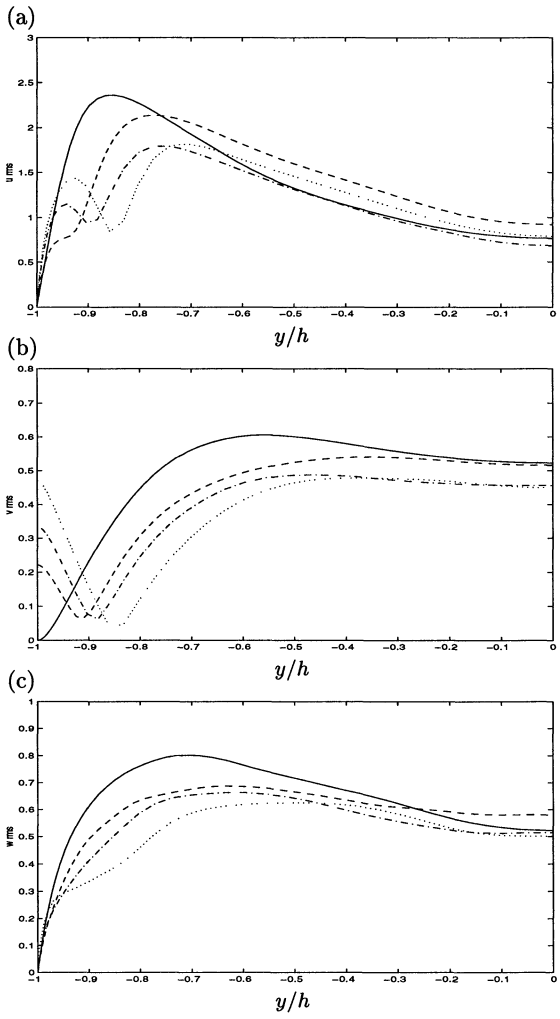


Figure 6: Turbulent intensities with different amplitude: (a) streamwise, (b) wall-normal, (c) spanwise component: solid, unmanipulated; dashed, $|C| = 1$; dash-dotted $|C| = 2$; dotted $|C| = 10$

peak becomes as large as the original near-wall maximum peak and they merge together, resulting in the substantial increase of the turbulence intensities and drag.

In Fig.6, turbulence intensities for three different control input amplitudes, $|C| = 1$, 2, and 10 are shown. In the streamwise component, one can clearly observe that the secondary peak becomes larger and the original one decays with the increase of amplitude, and that these peaks remain separated. This minimum in the streamwise intensity can be observed at nearly the same distance from the wall as that of the wall-normal component. This can be explained by employing the concept of a "virtual wall" (Hammond et al. 1998). In the opposing control case, this plane which has a minimum of through-flow can be seen halfway between the detection plane and the wall. As the amplitude becomes larger, this virtual wall is shifted towards the detection plane, resulting in a very small through-flow and low turbulence intensities, especially in the wall normal component.

The opposing control with $Y^+ = 15$ at the higher Reynolds number, $Re_c = 3300$, shows almost the same behavior in time histories and statistics. The friction Reynolds number, $Re_\tau$ decreases from 182 to 157 in a short time after the control input, whereafter it tends to the stable value around 162, resulting in a drag reduction about 20 %, which is smaller than that at $Re_c = 1800$. This is considered to be due to the fact that larger structures, which can be reduced by this control, are more dominant in the flow with lower Reynolds number. The mean velocity profiles in Fig.

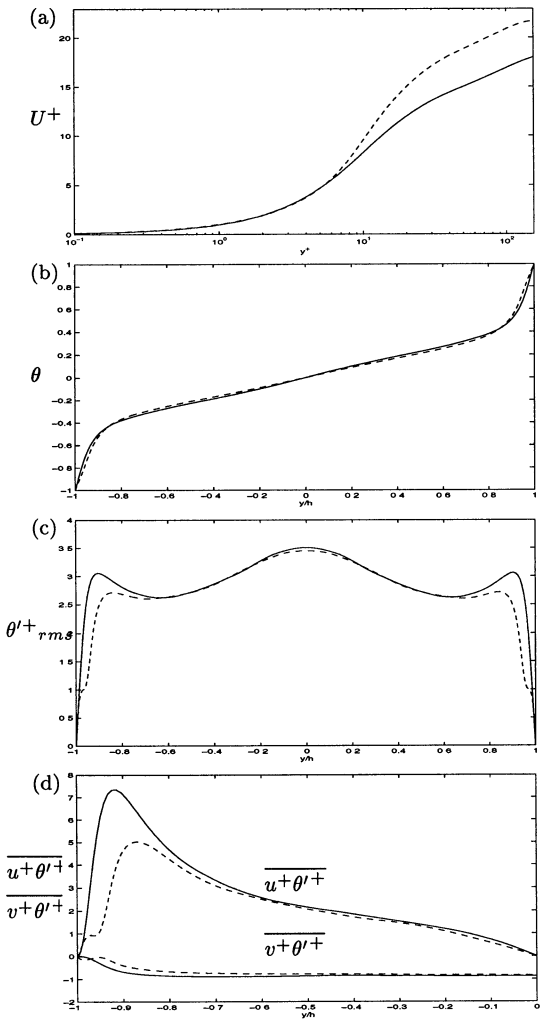


Figure 7: (a): Mean velocity; (b): Mean temperature; (c): Temperature intensity; (d): Heat fluxes; solid line, unmanipulated; dashed line, opposing control at $Y^+ = 15$, with $Re_c = 3300$

7(a), normalized by the actual friction velocity of each case, show a substantial upward shift of the controlled case, i.e. a substantial thickening of the viscous sublayer. For the mean temperature profile, the change is not so clearly detectable, but the derivative value at the wall signifies a reduced heat transfer as an effect of the control. The fact that the control is effective only close to the wall is also signified by a strong reduction in heat fluxes in the vicinity of the wall (Fig. 7(d)).

The contour plot of enstorophy, which is closely related with coherent structure is shown. Fig. 8(a) for the unmanipulated case and Fig.8(b) for the opposing control case with $Y^+ = 15$ at a Reynolds number $Re_c = 3300$ for both cases. It can be inferred that in the unmanipulated case, the coherent structures appear quasi-periodically in the spanwise direction, and that

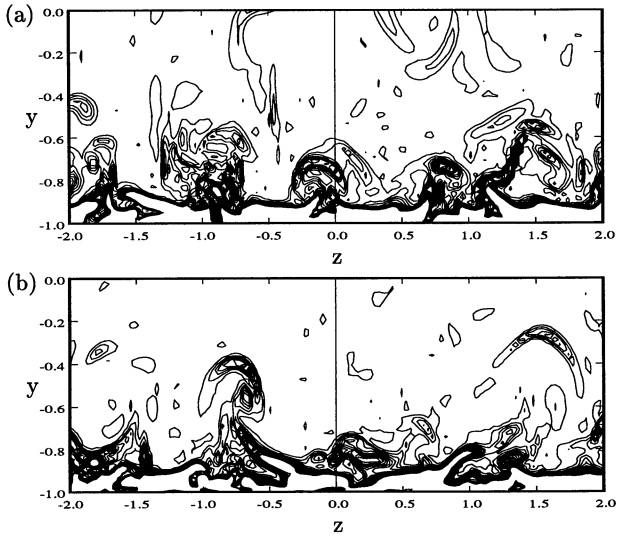


Figure 8: Contour plot of enstrophy $\overline{\omega_i\omega_i}$ , normalized with $U_c$ and h, in a cross flow plane. The contour levels range from 0 to 30 by increments of 2. The plot domain extends from the lower wall to the center of the channel in wall-normal direction. (a) Unmanipulated ,(b) Opposingly controlled at $Y^+ = 15$ with $Re_c = 3300$.

these strong events have been substantially attenuated by the control. This illustrates the fact that this control scheme mainly acts to reduce the strong events. In addition, the vortex structures are moved outward from the walls, introducing the outward shift of turbulence and passive scalar intensities.

By shifting the detection plane outward from the wall after an initial control period, the drag temporarily decreased for a short time period after the shift of the detection plane (shown Fig.9). The lower Reynolds number $Re_c = 1800$ was again employed in this calculation with the control input $Y^+ = 15$, $|C| = 10$, $\Theta = \Pi$ until t=400. At t=400, the detection plane was shifted to $Y^+ = 20$ with the rest of the parameters fixed as before. At the instance of the shift, the drag first increased whereafter it decreased until reaching a minimum of $Re_\tau \approx 76$ around $t \approx 600$. Thereafter it increased again to a value around $Re_\tau = 87$. The further plane shift over $Y^+ = 20$ did not lead to any drag reduction.

It has been shown that the coherent structures are attenuated with this control scheme. One may be able to produce the coherent structures by imposing sinusoidal blowing and suction control input from the walls with suitable amplitude and frequency, which may make it possible to position the structures more effectively at a desired distance from the wall. This will be an interesting task for the near future.

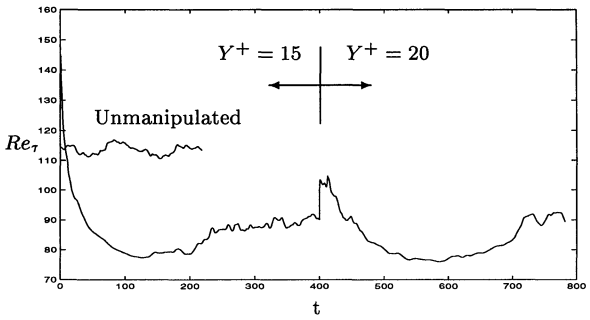


Figure 9: Time history of the friction Reynolds number with the detection plane, at $Y^+ = 15$ until t=400, and $Y^+ = 20$ thereafter with $|C| = 10$, and $\Theta = \Pi$ fixed throughout the calculation

## CONCLUSION

An active feedback control scheme with blowing and suction from the channel walls was tested with various input parameters, and proved to perform fairly well to get up to 30 % drag reduction for some successful cases. This control scheme mainly acts to suppress the strong events, i.e. large vortex structures, and displacing them outward from the wall.

## REFERENCE


Choi, H., Park, J., and Hahn, S., 1997, "Effects of blowing/suction from a spanwise slot on a turbulent boundary layer flow," *11th turbulent sheer flows*, Vol. 1, P1-37.

Choi, H., Moin, P., and Kim J., 1994, "Active turbulence control for drag reduction in wall-bounded flows," *J. Fluid Mech*, Vol. 262, pp. 75-110.

Farrell, F., B., and Ioannou, J., P., 1996, "Turbulence suppression by active control," *Phys. of Fluids*, Vol. 8, No. 5, pp. 1257-1268. Hammond, P., E., Bewley, R., T., Moin, P., 1998, "Observed mechanisms for turbulence attenuation and enhancement in opposition-controlled wall-bounded flows," *Phys. of Fluids*, Vol. 10, No. 9, pp. 2421-2423.

Kasagi, N., Sumitani, Y., Suzuki, Y., and Iida, O., 1995, "Kinematics of the quasi-coherent vortical structure in the near-wall turbulence," *Int. J. Heat and Fluid Flow*, Vol. 16, No. 1, pp. 2-10.

Kim, J., Moin, P., and Moser, R., 1987, "Turbulence statistics in fully developed channel flow at low Reynolds number," *J. Fluid Mech*, Vol. 177, pp. 133-166.

Lee, C., Kim, J., and Choi, H., 1998, "Suboptimal control of turbulent channel flow for drag reduction," *J. Fluid Mech*, Vol. 358. pp. 245-258.

Satake, S., and Kasagi, N., 1997, "Suboptimal turbulence control with the body force of selective velocity damping localized to the near-wall region," *11th turbulent sheer flows*, Vol. 1, P1-43.

Sumitani, Y., and Kasagi, N., 1995, "Direct Numerical Simulation of Turbulent Transport with Uniform Wall Injection and Suction," *AIAA Journal*, Vol. 33, No. 7, pp. 1220-1228.